

Integration and testing of FTS-2: an imaging Fourier transform spectrometer for SCUBA-2

Brad Gom^{*a}, David Naylor^a, Baoshe Zhang^a

^aDepartment of Physics, University of Lethbridge, Lethbridge, Alberta, Canada, T1K 3M4

ABSTRACT

FTS-2 is an imaging Fourier transform spectrometer (IFTS) being developed for use with SCUBA-2, the second generation, wide-field, submillimetre camera which will operate at the James Clerk Maxwell Telescope (JCMT). The FTS-2 interferometer uses a folded Mach-Zehnder configuration and will provide simultaneous broadband spectral imaging across both the 850 and 450 μm bands with variable resolution ranging from resolving powers of $R \sim 10$ to 5000. Details of the instrument design, optical modeling, data reduction pipeline and calibration plan which have changed since the project CDR are discussed, along with preliminary results of lab integration and testing.

Keywords: Fourier, Spectrometer, SCUBA-2, Submillimetre, JCMT

1. INTRODUCTION

An imaging spectrometer, named FTS-2, is currently under development to extend the capabilities of the recently installed SCUBA-2 bolometer camera¹ on the JCMT. Lab integration and testing of FTS-2 is expected to be completed by the end of 2008, with installation and commissioning at the JCMT taking place in 2009 after SCUBA-2 is commissioned. Previous papers have discussed the preliminary design² and observing modes^{2,3} of FTS-2. In this paper we review the system design as the project enters the final construction phase. The optical design of the interferometer and modeled performance is presented in a separate paper⁴.

2. MECHANICAL DESIGN

The mechanical framework design described previously² has evolved into a modular system as shown in Fig. 1. This approach allows the optics in the various modules (the folding mirrors in the interferometer arms, the beamsplitters, the pickoff mirrors, and the moving mirror assembly) to be aligned and mounted separately to the optical breadboard, and also reduces manufacturing cost. The framework components are manufactured from Mic-6® aluminum tooling plate⁵ which has excellent flatness and distortion characteristics. Positional tolerances for the optics⁴ within each module can be achieved by doweling of the framework plates; alignment of the modules to one another will be achieved using a coordinate measuring machine before the modules are bolted to the optical breadboard. Once the framework components are positioned, they will be located with mechanical stops to allow the interferometer to be disassembled for shipping since the entire instrument is too large to ship as a unit (mass ~ 600 kg, volume $\sim 2\text{m} \times 0.6\text{m} \times 1.3\text{m}$).

The framework is designed to avoid interference with the SCUBA-2 beam and the JCMT telescope backing structure while maintaining high rigidity for resistance to vibration. There is sufficient space around all the components to allow for a reasonable amount of flexibility in the design; stiffness can be increased as necessary by adding suitable bracing or increasing thickness. The framework will have sufficient stiffness to maintain the mirrors within the optical tolerances ($\sim \pm 200 \mu\text{m}$) and ensure that resonant frequencies are kept above 400 Hz.

Another design modification was the inclusion of blackbody calibration shutters in both arms of the interferometer, as shown in Fig. 2. These motorized shutters can be inserted in front of the input beamsplitter so that the interferometer can be operated in a single-input mode for testing purposes, and also to characterize the instrumental phase. The blackbody surfaces will not be temperature controlled, but will incorporate temperature sensors for calibration.

The FTS-2 framework is currently being manufactured. The pickoff mirror unit (Fig. 3) and moving mirror assembly (Fig. 4) have been built and tested. Alignment precision and repeatability are within the optical tolerancing specifications.

* brad.gom@uleth.ca; phone 1 403 329-2771; fax 1 403 329-2057; <http://research.uleth.ca/scuba2/>

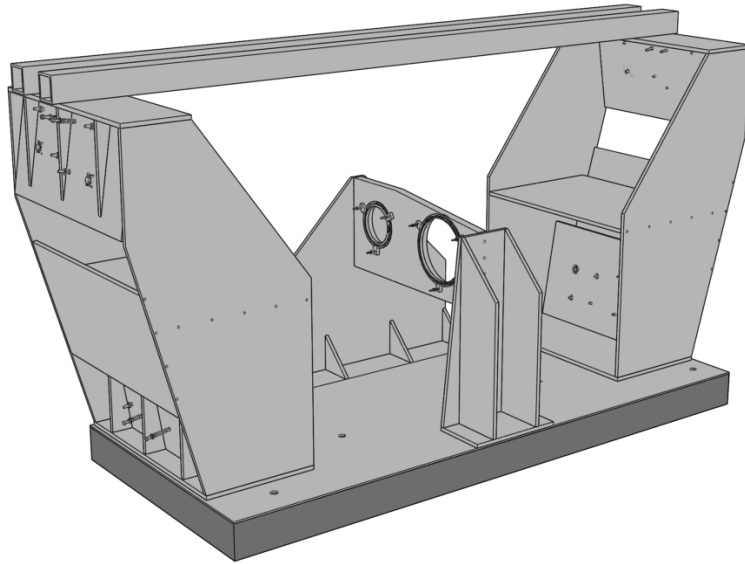


Fig. 1. Mechanical framework of the FTS-2 instrument; optics and mechanisms are omitted for clarity. A tower at each end of the instrument houses the 4 folding mirrors for each arm of the interferometer. Mirror mounts are integrated into the framework components.

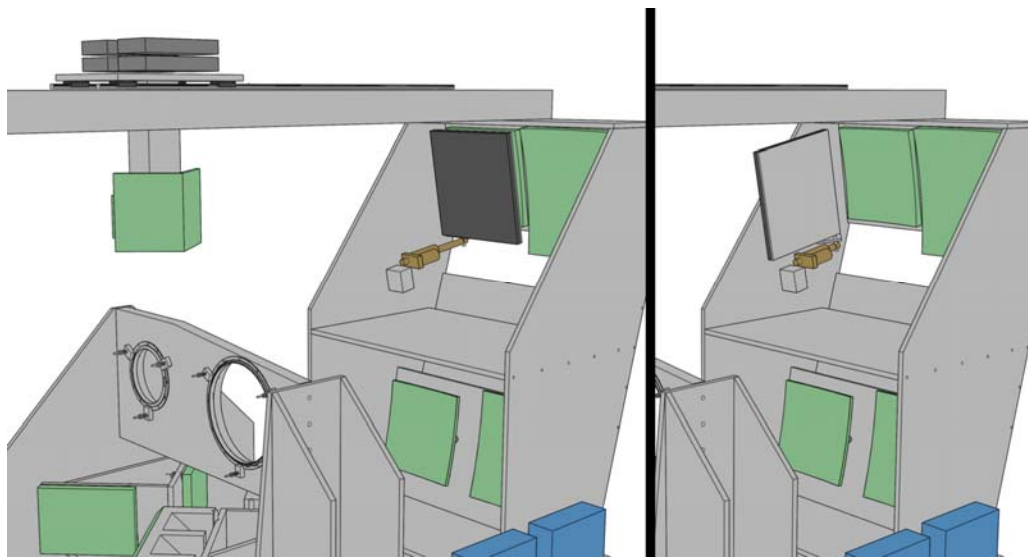


Fig. 2. Calibration blackbody shutters are included in both input ports of the interferometer, and can be inserted (left) or removed (right) from the beam when required using a motorized actuator.

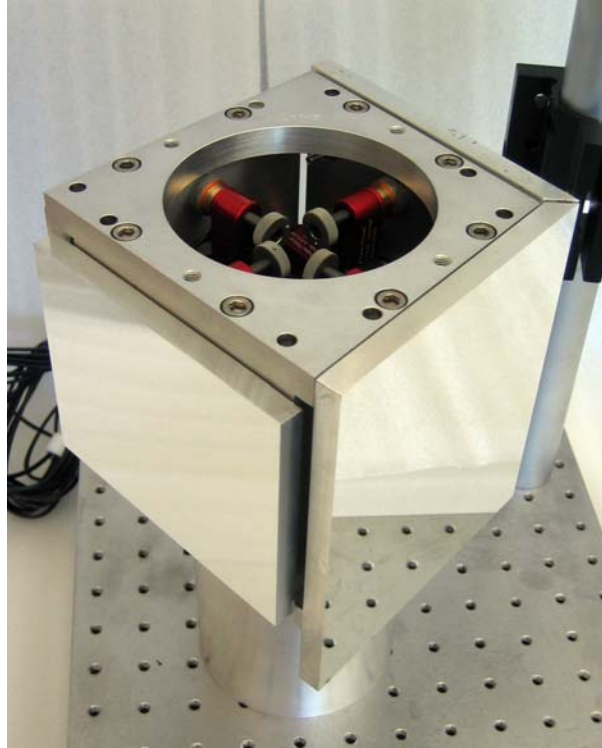


Fig. 3. The pickoff mirror assembly, showing 4 of the 8 internal piezo alignment actuators and the diamond-turned aluminum mirrors. The two input mirrors on the left are smaller than the output mirrors on the right due to the diverging telescope beam at the FTS-2 mounting location. The assembly is inverted when installed on the instrument.

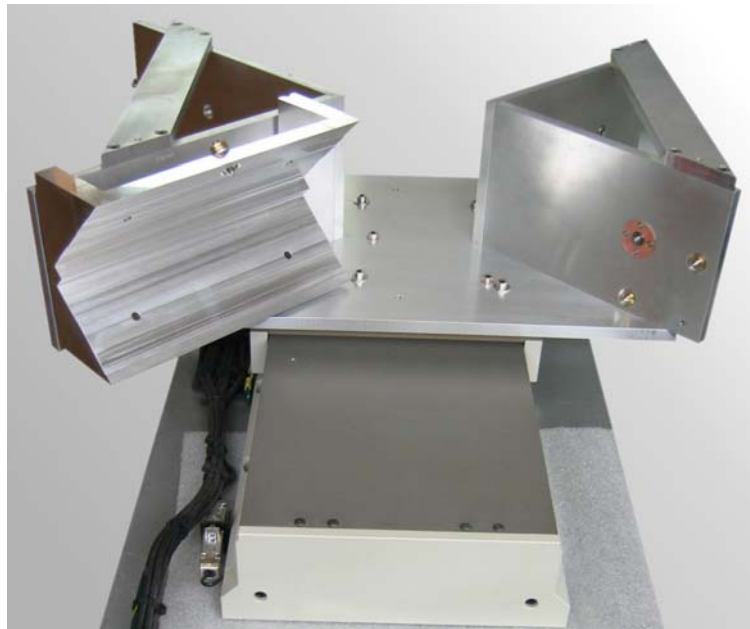


Fig. 4. Moving mirror assembly shown installed on the translation stage. The rooftop portion of the corner-cube retroreflectors (left side) are formed by two pairs of flat diamond-turned aluminum mirrors; the remaining mirrors of the corner-cubes are mounted on spherical bearings with tip/tilt adjustment (right).

Mirror mounts for FTS-2 represent a special challenge, due to the space constraints and optics sizes. The pickoff mirror assembly incorporates spherical bearing based mounts in order to support the mirror mass while minimizing radial loading on the piezo actuators. Spherical bearings are also used in the plane mirror portion of the moving corner cube mirrors, but since the tolerances for the rear surfaces of the aspherical freeform mirrors in the interferometer arms is not controlled, simple kinematic mounts with adjustability in all six degrees of freedom are used.

3. OPTICS

Detailed results of the optical modeling and theoretical optical performance are presented elsewhere⁴; in this section we present a summary of the imaging performance of the interferometer and measured performance of the FTS-2 beamsplitters.

3.1 Imaging Performance

The maximum field of view of the FTS input ports is ultimately limited by the maximum practical mirror sizes (roughly 400 mm diameter) to approximately 5 arcmin². The system maintains diffraction limited spot sizes at intermediate spectral resolution (mirror travel up to ~100 mm). The computed fraction of rays passing through the FTS unvignetted and the interferogram contrast ratio for the central field are given in Table 1, as a function of mirror travel for low, medium, and high spectral resolution. For the outer field points, the corresponding values are given in Table 2.

Table 1. Efficiency of FTS-2 for the central field considering vignetting losses as a function of mirror travel.

Travel Distance	Fraction of Rays Passing Through FTS		Interferogram Contrast
	Positive Travel Side	Negative Travel Side	
ZPD	88.99%	88.99%	1.000
±15mm	89.80%	88.07%	0.981
±100mm	95.46%	83.53%	0.875
±200mm	98.27%	80.32%	0.817

Table 2. Efficiency of FTS-2 for the outer field considering vignetting losses as a function of mirror travel.

Travel Distance	Fraction of Rays Passing Through FTS		Interferogram Contrast
	Positive Travel Side	Negative Travel Side	
ZPD	90.77%	90.77%	1.000
±15mm	86.69%	91.94%	0.943
±100mm	39.21%	65.68%	0.597
±200mm	3.37%	10.91%	0.309

3.2 Beamsplitter Performance

At submillimeter wavelengths, atmospheric emission dominates the signal from the astronomical source, even when observing from high mountain sites. Moreover, variations in atmospheric emission are particularly problematic for an FTS because, upon transformation, they introduce artifacts into the resulting spectrum. By utilizing the second input port of FTS-2 to view an adjacent background sky position, variations in atmospheric emission can, to first order, be cancelled by the subtractive properties of an FTS. Moreover, this cancellation results in a dramatic reduction in the dynamic range required in the resulting interferogram.

During the performance evaluation of the SPIRE spectrometer of the Herschel Space Observatory⁶, which shares a similar design to FTS-2, it has been shown that beamsplitter emission can contribute significantly to the measured interferogram when port balancing is optimum⁷. This is of concern to FTS-2 since it not only introduces a systematic modulated signal, but one that is out of phase with the astronomical signal⁸ by $\sim\pi/2$, and therefore one that must be removed prior to phase correcting the measured interferogram – an important step in the data processing pipeline.

Many types of beamsplitters have been used in far infrared FTS ranging from the standard dielectric film (usually Mylar), inductive metal mesh and polarizers (free standing wires or metal strips deposited on a thin substrate). Dielectric and metal mesh beamsplitters have a limited spectral range and typical efficiencies (4RT) of 60% and 75%, respectively. By comparison, the polarizer affords a high efficiency over a broad spectral range, but allows detection of only one polarization component of the source.

Extending on previous work in the development of far infrared metal mesh filter technology⁹, a new beamsplitter has been developed which possesses both a high and uniform efficiency over a broad spectral range and is insensitive to source polarization. This design uses two metal meshes in a Fabry-Perot configuration designed to meet the 50:50 reflection/transmission criteria of an ideal beamsplitter¹⁰. The geometry of the complementary structures of capacitive and inductive grids determines the precise spectral range of the beamsplitter, whose development has evolved along two independent paths. In the first, the complementary structures are deposited on two thin Mylar substrates, which are held parallel to each other and separated by a precision air gap. In the second, the structures are deposited onto polypropylene substrates and bonded together in a hot press process; both designs have been shown to be effective as beamsplitters. The hot pressed design, however, is less sensitive to vibration and thus preferred for the hostile environment encountered at the JCMT.

A study was therefore undertaken to evaluate the magnitude of the emission from the two beamsplitter designs to determine if there was any optical advantage in the air gap design which employs less dielectric material. Resistive losses in the deposited metal structures are responsible for absorption in the beamsplitter, and subsequent emission. This absorption limits the attainable finesse and ultimate efficiency of the Fabry-Perot cavity, but is known to be small for the simple metallic grid structures employed.

Identical blackbody sources were placed at the two input ports of a Mach-Zehnder FTS¹¹ of similar design of FTS-2. One of the sources was maintained at a temperature of 30°C while the other was heated to 33°C and allowed to cool to 27°C; interferograms were obtained approximately every minute as the source cooled. The left panels in Fig. 5 shows the zero path difference region of the interferograms corresponding to temperature differences between the two input ports of approximately 0 (optimal nulling) and +/- 1 K when using the hot pressed (top) and air gap (bottom) beamsplitters. When the beamsplitter emission component is subtracted from the two other measurements, the complementarity of the port dominant signals is evident (right panels); at this point standard phase correction procedures can be invoked.

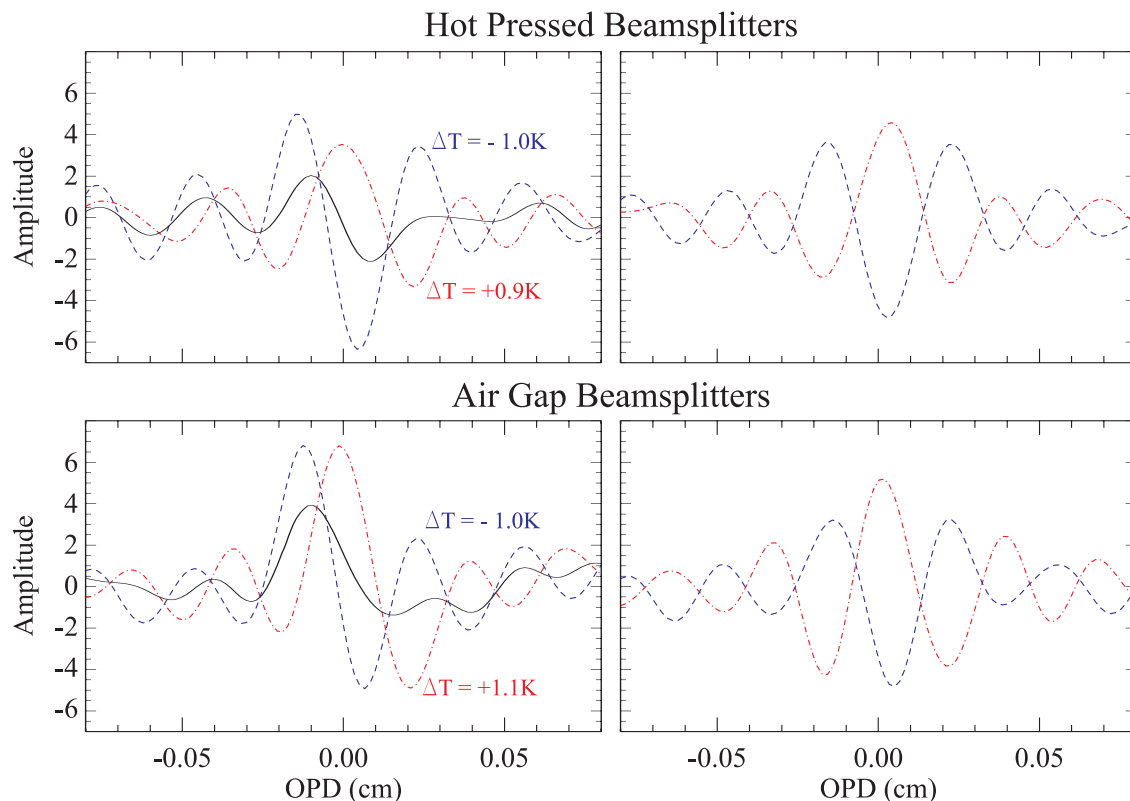


Fig. 5. Comparison of the zero path difference regions of interferograms measured using hot pressed (top) and air gap (bottom) beamsplitters. Interferograms measured with a +1K temperature difference between the input ports are shown with dash-dot lines; interferograms with a -1K difference between the input ports are shown with dotted lines. When both input sources are the same temperature, a null interferogram (solid lines) is recorded which represents the beamsplitter emission. The right panels show the original interferograms after the null interferogram is subtracted.

The study of the beamsplitter emission contribution to the interferogram observed with a Mach-Zehnder interferometer has shown that the effect is non-negligible and that the data processing pipeline for FTS-2 must take this into account. On the positive side, the emission term does not depend on the fabrication process; this is what one would expect if the absorption was due to a resistive component in the metal grids and not the dielectric substrates, as the deposition mechanism is the same for both beamsplitter types. As a result, the hot pressed design has been adopted for FTS-2.

4. ATMOSPHERIC CANCELLATION

FTS-2 has two input ports with fixed angular separation. For any observation, one port is aligned with the object of interest and the second (background) port rotates in an arc about the tracking center as a consequence of sky rotation due to the Alt-Az telescope. Details of the port geometry can be found in the companion paper⁴. Since pixels in both ports will rotate about the tracking center during long observation sequences, and since the differencing is done optically in the interferometer, pixels in both ports will experience different and varying flux due to the slight atmospheric imbalance. Consequently, a good model of the behavior of the ports, and of the extent of the atmospheric flux difference as a function of elevation and time, is crucial for planning and interpreting FTS-2 observations.

The atmospheric emission and the orientation of the FTS-2 input ports have been modeled for a range of astronomical targets and atmospheric conditions. Since the sky rotation is slow relative to the acquisition time for an individual interferogram, only the instantaneous flux difference between the two ports was calculated. Temporal variations in atmospheric emission between the two ports will also occur, but this is less significant and can only be characterized during instrument commissioning at the telescope. Fig. 6 shows the possible orientations of the FTS-2 ports when observing a region of the Taurus molecular cloud, over the period of time that the source is observable.

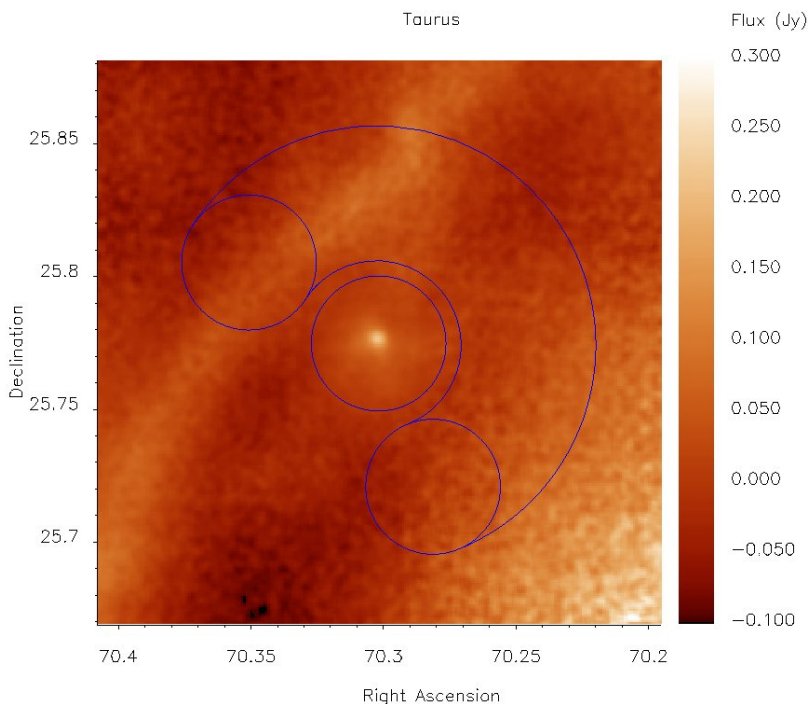


Fig. 6. SCUBA image¹² of a region of the Taurus molecular cloud with the FTS-2 input port trajectories superimposed. Port 1 is centered on the target, while Port 2 sweeps out an arc as a function of source elevation and time. The output of the interferometer is the interferometric difference of the two input ports.

An atmospheric radiative transfer model, BTRAM¹³, was used to calculate the atmospheric emission over the 450 and 850 μm bands (21.1 to 23.5 cm^{-1} and 11.2 to 12.1 cm^{-1} , respectively) for elevations ranging from zenith to 70° in $\sim 0.1^\circ$ increments, and for PWV values of 0.5 and 1 mm. The resulting spectral cubes were interpolated with a cubic spline at the elevation values calculated for each pixel at a given port orientation. The mean BTRAM spectral radiance across the band was then converted to flux in Janskys using a 7 arcsec beam size for the 450 μm band and 14 arcsec for the 850 μm band.

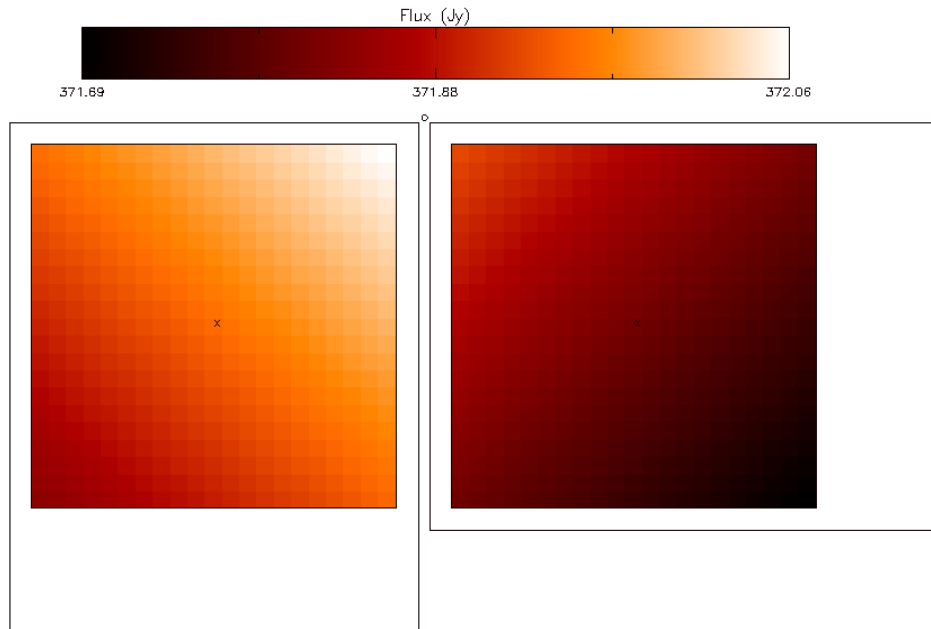


Fig. 7. Atmospheric emission as seen by the two FTS-2 input ports at 850 μm and an elevation of $\sim 40^\circ$. The FOV for the two corresponding SCUBA-2 detector subarrays are shown as the larger rectangles; the telescope optical axis is indicated by the small o. Note that the FTS-2 images are flipped and rotated relative to the normal SCUBA-2 images.

When the difference between the two input ports is taken, the resulting imbalance is always a horizontal gradient across the arrays (in the detector image plane), as seen in Fig. 8. This is a consequence of the unique geometry of FTS-2 which mirrors the FTS output ports horizontally across the centers of the ports. The imbalance is always most favorable near the telescope axis, and worse at the outer edge of the FOV, for all elevations. This can be seen in Fig. 9, where the imbalance for 0.5mm PWV is plotted as a function of zenith angle for 3 points along the horizontal axis through the center of the ports.

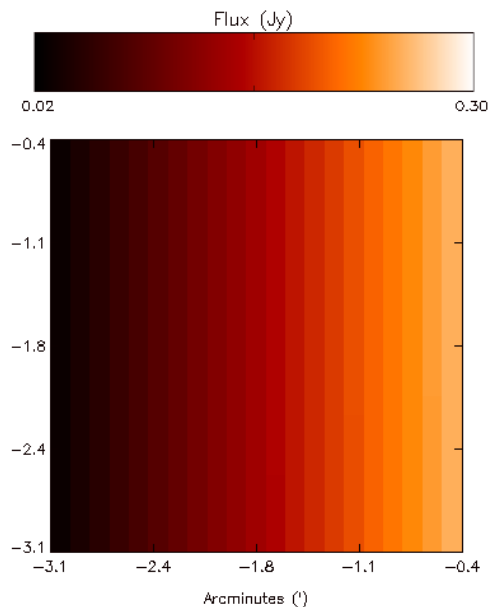


Fig. 8. The difference of the two input ports produces a residual horizontal gradient across the FTS-2 output ports, with amplitude that varies slowly with elevation. While the residual flux is still comparable to that of many sources, it can be easily modeled and the gradient can be subtracted during data processing.

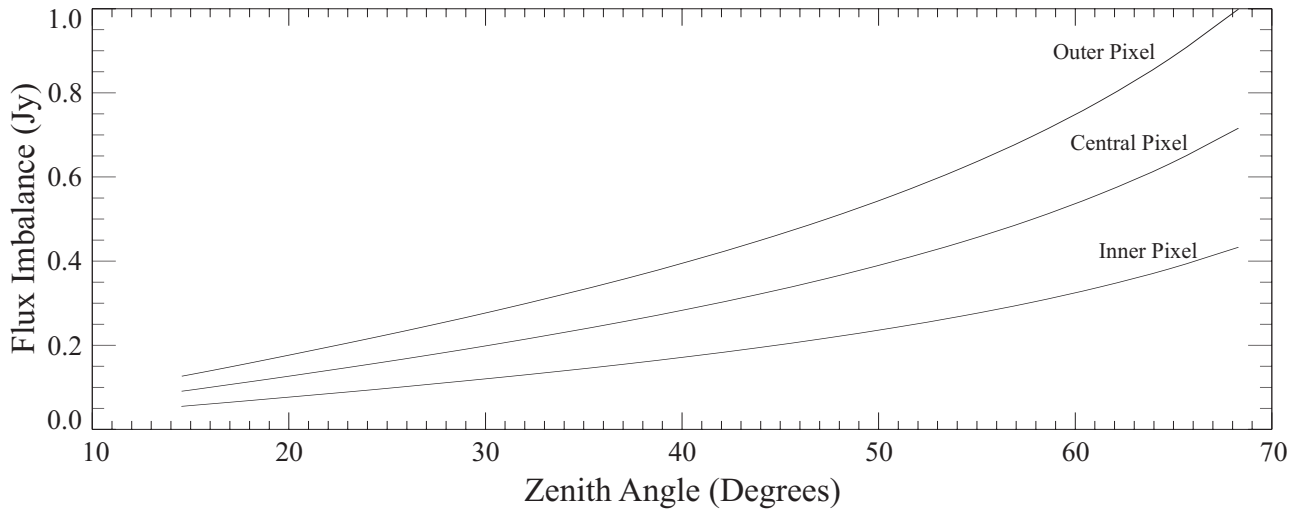


Fig. 9. Flux imbalance between the two input ports as a function of zenith angle for 3 pixels on the horizontal axis through the center of the ports, at 0.5mm PWV. The innermost pixels always have the smallest angular separation on the sky for any given elevation, and thus the smallest imbalance.

While the final sensitivity of FTS-2 will only be known following commissioning of FTS-2 after the scientific grade SCUBA-2 bolometer arrays are installed, current models predict that a spectral sensitivity of ~ 50 mJy per resolution element of 3 GHz (0.1 cm^{-1}), 5σ per hour, in the $850 \mu\text{m}$ band, will be achieved. The spectral sensitivity in the $450 \mu\text{m}$ band is typically much worse, being heavily dependent on the poor transmission of this atmospheric window; models predict an equivalent spectral sensitivity of ~ 250 mJy per resolution element. In order to reach these sensitivity limits, the systematic gradients resulting from the remnant atmospheric flux imbalance (shown in Fig. 8) must be removed during post processing.

5. SOFTWARE

All FTS-2 internal mechanisms are controlled over Ethernet by a control computer which interacts with the JCMT Observatory Control System (OCS)¹⁴ and Real Time Sequencer (RTS)¹⁵ in order to provide integration with the observatory software and synchronization with the telescope and SCUBA-2 systems.¹ Interferograms are recorded by the SCUBA-2 Data Acquisition system at the normal 200 Hz framerate, and the FTS-2 moving mirror motion controller records the mirror position synchronously with each frame. An overview of the FTS-2 mechanisms and control communication is shown in Fig. 10.

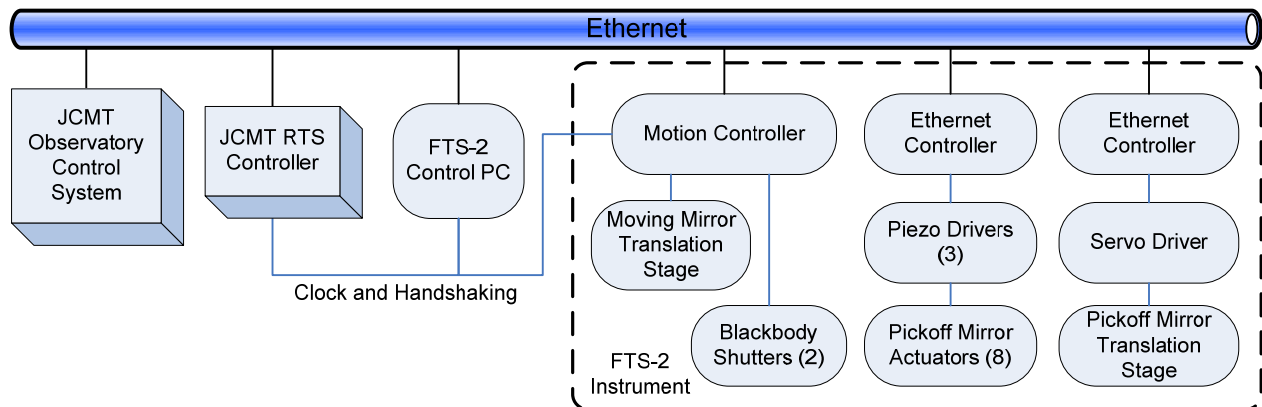


Fig. 10. Schematic of FTS-2 mechanisms and control system.

The SCUBA-2 data reduction pipeline¹⁶ is written in object-oriented Perl and uses algorithm engines for the bulk of the algorithmic data processing. Since the implementation of the algorithm engines is independent of the pipeline itself, the FTS-2 algorithm engine has been written in Java to exploit existing Herschel SPIRE code¹⁷ written by members of our group. The FTS-2 engine uses a Java version of FFTPack¹⁸ (translated from the original FORTRAN code by the FTS-2 group) for fast Fourier transforms of the interferogram data.

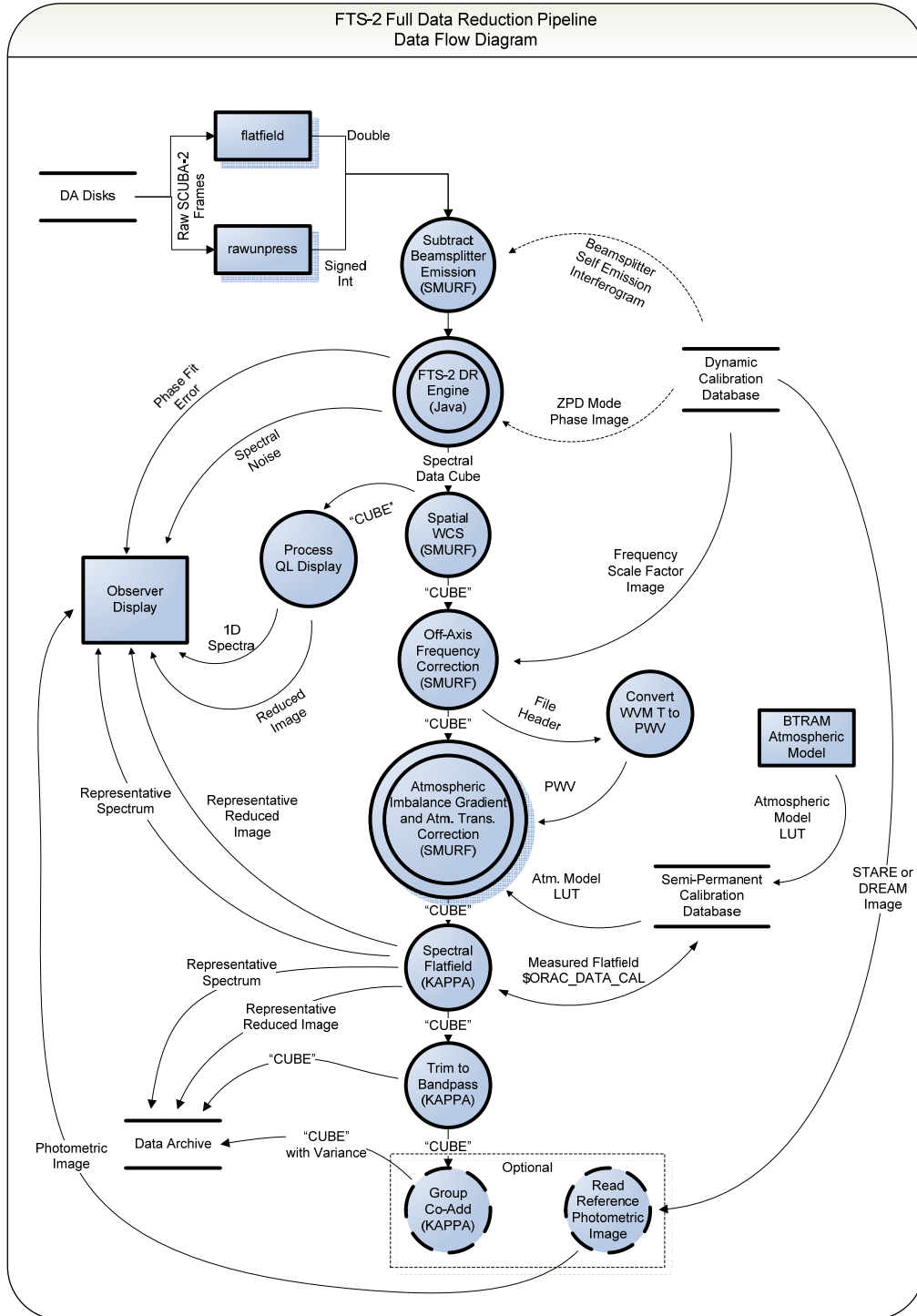


Fig. 11. Data flow diagram for the FTS-2 data reduction pipeline.

As shown in Fig. 11, the pipeline first combines the SCUBA-2 frames and FTS mirror position values into interferograms, subtracts the beamsplitter self-emission calibration interferogram, and then passes the interferogram cubes to the FTS-2 Java data reduction engine. The Java engine removes cosmic ray glitches, corrects the asymmetry of an interferogram (so that a single-sided transform may be used), resamples the interferograms onto an even OPD grid (allowing use of the FFT algorithm), applies a phase correction function, and then calculates a spectral data cube. Using infrastructure of the SCUBA-2 pipeline, the spatial coordinate system is applied to the data files and the frequency scale is corrected for the intrinsic FTS obliquity effect¹⁹. The spectra are corrected for the residual atmospheric emission gradient and the atmospheric transmission as calculated from an atmospheric model for the measured water vapor content. Spectral data cubes are then stored in the normal SCUBA-2 data archive. A simplified ‘Quick Look’ display system will display partially processed spectra in real time at the telescope.

6. CONCLUSION

The current status of FTS-2, the imaging spectrometer for SCUBA-2, has been reviewed as the project enters the final construction phase. A comparison of competing beamsplitter technologies has shown that the hot pressed design is better suited for FTS-2. However, the beamsplitter emission is observable and the data processing pipeline has been updated to remove this effect. Modeling of the atmospheric cancellation expected with the dual input port design shows that it should be relatively straightforward to remove the residual atmospheric gradient from spectroscopic measurements with FTS-2. Laboratory integration and testing is underway and is expected to be completed by the end of 2008, with installation and commissioning at the JCMT set to take place in 2009, after SCUBA-2 has been commissioned.

7. ACKNOWLEDGEMENTS

On behalf of the Canadian SCUBA-2 consortium, the authors acknowledge the support of a CFI international access award for Canadian participation in the SCUBA-2 project. David Naylor acknowledges support from NSERC. The authors also acknowledge the work of Alison Faulkner and David Rotenberg in modeling the atmospheric emission cancellation for FTS-2, Peter Ade and Carole Tucker for providing the beamsplitters, and Locke Spencer for his contributions to the beamsplitter emission measurements.

REFERENCES

1. Holland, W.S., Duncan, W.D., Kelley, B.D., Irwin, K.D., Walton, A.J., Ade, P.A.R., and Robson, E.I., “SCUBA-2: A large format submillimetre camera on the James Clerk Maxwell Telescope”, *Proc. SPIE, Millimeter and Submillimeter Detectors for Astronomy* **4855**, 1-18 (2003).
2. Naylor, D.A., Gom, B.G., Zhang, B., “Preliminary design of FTS-2: an imaging Fourier transform spectrometer for SCUBA-2”, *Proc. SPIE, Astronomical Telescopes and Instrumentation* **6275**, (2006).
3. Naylor, D.A., Gom, B.G., Fulton, T.R., Tahic, M.K., and Davis, G.R., “Increased Efficiency through Undersampling in Fourier Transform Spectroscopy”, *Optical Society of America, FTS topical meeting*, Alexandria, Virginia, (2005).
4. Naylor, D.A., Gom, B.G., Leclerc, M.R., “Optical design of the SCUBA-2 IFTS”, *Proc. SPIE, Millimeter and Submillimeter Detectors and Instrumentation for Astronomy* **7020**, (in press).
5. Alcoa North America, 4879 State St., P.O. Box 8001, Bettendorf, IA 52722-8001.
6. Spencer, L.D., Naylor, D.A., Zhang, B., Davis-Imhof, P., Fulton T.R., Baluteau, J.-P., Ferlet, M. J., Lim, T.L., Polehampton, E.T. and Swinyard, B.M., “Performance evaluation of the Herschel/SPIRE instrument flight model imaging Fourier transform spectrometer,” *Proc. SPIE, Space Telescopes and Instrumentation I: Optical, Infrared, and Millimeter Wave* **7010**, (in press).
7. Spencer, L.D., Naylor, D.A., Fulton, T.R., Baluteau, J.P., Ade, P.A.R., Davis, P.W., and Swinyard, B.M., “Port Compensation Using the Herschel/SPIRE Imaging Fourier Transform Spectrometer”, *Proc. IRMMW, THz and MMW Applications in Astronomy, Atmospheric and Environmental Science*, Cardiff, U.K., 718-719 (2007).
8. Carli, B., Palchetti, L., and Raspollini, P., “Effect of beam-splitter emission in Fourier-transform emission spectroscopy”, *Applied Optics* **38**, 7475-7480 (1999).

9. Lee, C., Ade, P.A.R., and Haynes, C.V., "Self Supporting Filters for Compact Focal Plane Designs", *Proc. of the 30th ESLAB Symposium*, ESTEC, Noordwijk, The Netherlands, (1996).
10. Ade, P.A.R., Hamilton, P.A., and Naylor, D.A., "An Absolute Dual Beam Emission Spectrometer", *Fourier Transform Spectroscopy: New Methods and Applications*, OSA, 90-92 (1999).
11. Naylor, D.A., Gom, B.G., Schofield, I.S., Tompkins, G.J., Davis, G.R. "Mach-Zehnder Fourier transform spectrometer for astronomical spectroscopy at submillimeter wavelengths", *Proc. SPIE, Millimeter and Submillimeter Detectors for Astronomy* **4855**, 540-551 (2003).
12. Di Francesco, J., Johnstone, D., Kirk, H., MacKenzie, T. & Ledwosinska, E., "The SCUBA Legacy Catalogues: Submillimeter-Continuum Objects Detected by SCUBA", *ApJS* **175**, 277 (2008).
13. BTRAM, <http://www.blueskyinc.ca>
14. Rees, N.P., Economou, F., Jenness, T., Kackley, R.D., Walther, C.A., Dent, W.R., Folger, M., Gao, X., Kelly, D., Lightfoot, J.F., Pain, I., Hovey, G., and Redman, R.O., "JCMT observatory control system", *Proc. SPIE, Advanced Telescope and Instrumentation Control Software II* **4848**, (2002).
15. Kelly, B.D., <http://www.roe.ac.uk/ukatc/projects/scubatwo/documents/software/sc2-sof-s200-026.pdf>
16. Jenness, T., Economou, F., Scott, D., Kelly, B.D., and Holland, W. S., "Preliminary design of the SCUBA-2 Data Reduction Pipeline", *Astronomical Data Analysis Software and Systems XIII, ASP Conference Series* **314**, (2003).
17. Ott, S., et al., "News from the Herschel Data Processing System", *Astronomical Data Analysis Software & Systems XVI, ASP Conference Series* **376**, (2007).
18. JFFTPack documentation. Available: <http://netlib.sandia.gov/fftpack/>
19. Fulton, T.R., Naylor, D.A., Baluteau, J-P., Griffin, M.J., Davis-Imhof, P., Swinyard, B.M., Lim, T.L., Surace, C., Clements, D., Panuzzo, P., Gastaud, R., Polehampton, E., Guest, S., Lu, N., Schwartz, A. and Xu, K., "The data processing pipeline for the Herschel/SPIRE Imaging Fourier Transform Spectrometer", *Proc. SPIE, Space Telescopes and Instrumentation I: Optical, Infrared, and Millimeter Wave* **7010**, (in press)